A Study on Unsteady Flow Characteristics and Lateral Force of Conventional Bell-type Nozzle

Sugimoto, Koichi
Department of Aeronautics and Astronautics : Graduate Student

Aso, Shigeru
Department of Aeronautics and Astronautics : Professor

出版情報：九州大学工学紀要. 63 (2), pp.107-122, 2003-06-26. 九州大学大学院工学研究院
バージョン：
権利関係：

Memoirs of the Faculty of Engineering, Kyushu University, Vol. 63, No. 2, June 2003

A Study on Unsteady Flow Characteristics and Lateral Force of Conventional Bell-type Nozzle

by

Koichi SUGIMOTO* and Shigeru ASO**

(Received April 2, 2003)

Abstract

A numerical study on unsteady flow characteristics of conventional bell-type nozzle has been conducted. In the computations axisymmetric full Navier-Stokes equations have been solved. AUSUM-DV scheme is used for convection terms. Central difference is used for viscous terms and LU-ADI scheme is used for time integration. Baldwin -Lomax turbulence model is also used in the computations. The nozzle configuration of a truncated perfect nozzle is selected for computations. The starting process of the nozzle is simulated numerically and unsteady flow characteristics and flow separation and reattachment of the flow are observed carefully. Quite unsteady flow patterns are observed and in the starting process and FSS (Free shock separation) pattern and RSS (restricted shock separation) pattern are also observed. The surface pressure distributions of RSS show locally higher pressure region might generate lateral force of the nozzle in the starting process when asymmetrical flow separation occurs.

Keywords: Numerical simulation, Bell nozzle, Lateral force, Computational fluid dynamics

1. Introduction

Recently the development of fully reusable launch vehicles are in progress mainly in United States and European countries. However, since the interval for the development of fully reusable launch vehicles is considered to be more than two decades, the development of new expedable rockets are also in progress due to strong demands for efficient and low cost space transportation systems in the short interval. On the development of new expendable rockets the development of new rockect engine is one of the most important key technologies. major nozzle configuration of rocket engine is bell-type nozzle, which is a kind of contour nozzle. It is known that some of the nozzle configurations show significant lateral force during starting or stopping process of the nozzle[1)2)3)]. Also the generation of significant lateral force of rocket nozzle in starting or stopping process of the nozzle flow had already been reported in SSME (Space Shuttle Main Engine) and Vulcain rocket engine because in

*Graduate Student, Department of Aeronautics and Astronautics
**Professor, Department of Aeronautics and Astronautics

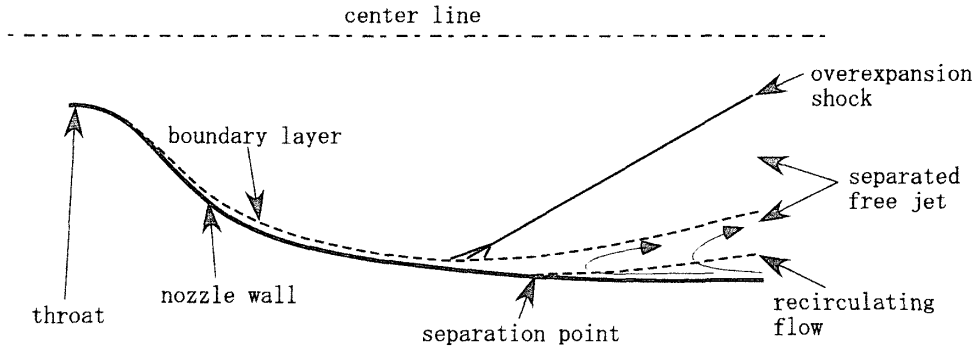

FSS : separated flow continues as a free jet

Fig. 1 Flow pattern of FSS (Free Shock Separation)

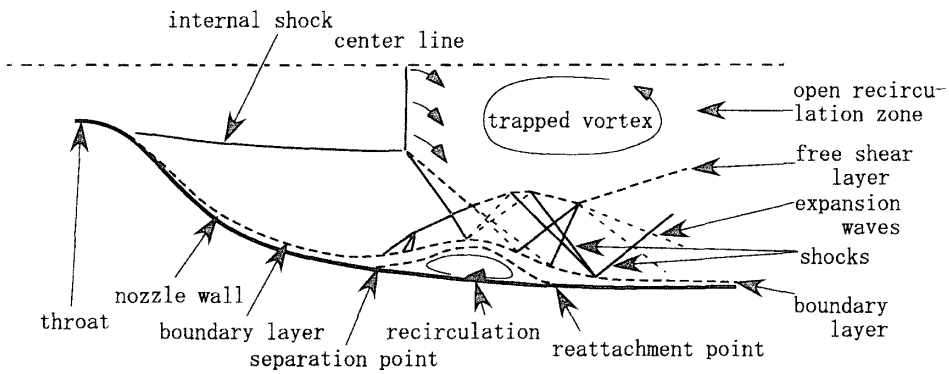

RSS : separated flow reattaches to the nozzle wall

Fig. 2 Flow pattern of RSS (Restricted Shock Separation)

the design process of the nozzle configurations of those rocket engines the main concern is located only in the steady flow conditions and quite few attention is paid for starting or stopping of the nozzle.

Frey and Hagemann[4] conducted numerical computations of flows in a conical nozzle and a nozzle proposed by Rao[6] and studied on separation position of the flow in nozzle and the parameter, which affects the separation point. Also in order to investigate the flow separation in the nozzle with over-expansion condition, numerical simulation was conducted by Onifri et. al.[1]. Their results show two flow patterns called FSS (Free Shock Separation) and RSS (Restricted Shock Separation) as shown in **Fig. 1** and **Fig. 2**. In FSS incoming flow separates due to adverse pressure gradient and after the separation an oblique shock wave and a re-circulating flow region are observed. In RSS condition internal shock wave and Mach disc, which are generated in the nozzle, interact each other and induce shock wave/boundary layer interaction. An incoming boundary layer separates and reattaches. Also a re-circulating flow region is formed between separation point and reattachment point. The pressure increase in the separated region of RSS is much higher than that of FSS and sometimes much higher than the ambient pressure.

Many researches had been conducted to reveal the mechanism of the generation of the significant lateral force. However, the detailed flow structure and flow mechanism have not been understood sufficiently.

2. Numerical Simulation

2.1 Governing Equations and Numerical Schemes

Governing equations are axi-symmetrical Navier-Stokes equations. In the present study AUSM-DV scheme is used for convection term, 2nd order central difference scheme is used for viscous term and LU-ADI scheme is used for time integration. Also Baldwin-Lomax turbulent model is used for turbulent modelling. Viscous coefficient is calculated by Sutherland's formula. At first two-dimensional Navier-Stokes equations are written as follows:

$$\frac{\partial Q}{\partial t}+\frac{\partial E}{\partial x}+\frac{\partial F}{\partial y}=0$$

$$Q=\begin{pmatrix}\rho\\ \rho u\\ \rho v\\ e\end{pmatrix}, E=\begin{pmatrix}\rho u\\ \rho u^2+p-\tau_{xx}\\ \rho uv-\tau_{xy}\\ (e+p)u-\tau_{xx}u-\tau_{xy}v-\kappa T_x\end{pmatrix}$$

$$F=\begin{pmatrix}\rho v\\ \rho uv-\tau_{yx}\\ \rho v^2+p-\tau_{yy}\\ (e+p)u-\tau_{yx}u-\tau_{yy}v-\kappa T_y\end{pmatrix}$$

By adding axi-symmetrical term, these equations are written as follows:

$$\frac{\partial Q}{\partial t}+\frac{\partial E}{\partial x}+\frac{\partial F}{\partial y}+H=\left(\frac{\partial E_v}{\partial x}+\frac{\partial F_v}{\partial y}+H_v\right)$$

$$Q=\begin{pmatrix}\rho\\ \rho u\\ \rho v\\ e\end{pmatrix}, E=\begin{pmatrix}\rho u\\ \rho u^2+p\\ \rho uv\\ (e+p)u\end{pmatrix} F=\begin{pmatrix}\rho v\\ \rho uv\\ \rho v^2+p\\ (e+p)v\end{pmatrix}$$

$$E_v=\begin{pmatrix}0\\ \tau_{xx}\\ \tau_{xy}\\ \tau_{xx}u+\tau_{xy}v+\kappa T_x\end{pmatrix} F_v=\begin{pmatrix}0\\ \tau_{yx}\\ \tau_{yy}\\ \tau_{yx}u+\tau_{yy}v+\kappa T_y\end{pmatrix}$$

$$H=\frac{1}{y}\begin{pmatrix}\rho v\\ \rho uv\\ \rho v^2\\ (e+p)v\end{pmatrix}, H_v=\frac{1}{y}\begin{pmatrix}0\\ \tau_{xy}\\ 2\mu(\frac{\partial v}{\partial y}-\frac{v}{y})\\ \tau_{yy}v+\tau_{yx}u+\kappa T_y\end{pmatrix}$$

κ is thermal conductivity and T_x and T_y are temperature gradients.

Stress tensors are written as follows:

$$\begin{pmatrix}\tau_{xx} & \tau_{xy}\\ \tau_{yx} & \tau_{yy}\end{pmatrix}=\mu\begin{pmatrix}2\dfrac{\partial u}{\partial x}-\dfrac{2}{3}\nabla\cdot u & \dfrac{\partial v}{\partial x}+\dfrac{\partial u}{\partial x}\\ \dfrac{\partial u}{\partial y}+\dfrac{\partial v}{\partial x} & 2\dfrac{\partial v}{\partial y}-\dfrac{2}{3}\nabla\cdot u\end{pmatrix}$$

and,

$$\nabla\cdot u=\frac{\partial u}{\partial x}+\frac{\partial v}{\partial y}+\frac{v}{y}$$

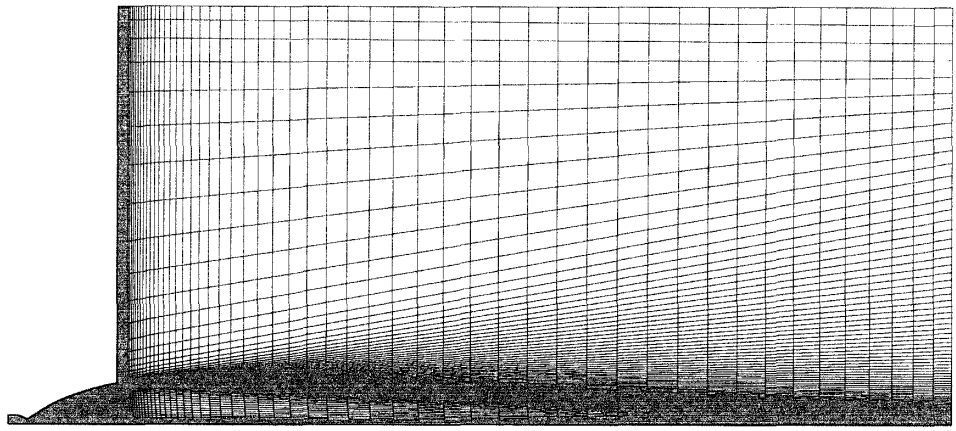

Fig. 3 Computational grid of bell-type nozzle

Then

$$\tau_{xx} = \frac{2}{3}\mu\left(2\frac{\partial u}{\partial x} - \frac{\partial v}{\partial y} - \frac{v}{y}\right)$$

$$\tau_{yy} = \frac{2}{3}\mu\left(-\frac{\partial u}{\partial x} + 2\frac{\partial v}{\partial y} - \frac{v}{y}\right)$$

$$\tau_{xy} = \tau_{yx} = \mu\left(\frac{\partial u}{\partial y} + \frac{\partial v}{\partial x}\right)$$

Sutherland's formula is written as follows:

$$\mu = C_1 \frac{T^{3/2}}{T + C_2}$$

and $C_1 = 1.458 \times 10^{-6}$ kg/(m · s · K$^{1/2}$), $C_2 = 110.4$ K.

2.2 Computational Grid

The computational grid used by this study is shown in **Fig. 3**. A configuration of a compressed truncated Perfect Nozzle[7] is selected as shown in the Figure. The full length of the nozzle is about 1.8 m. Expansion ratio of the nozzle is about 50. In the numerical simulations the inner flow region of the nozzle and the outer flow region of the nozzle are solved simultaneously. The width and the height of an outside computational domain are 20 times and 10 times of the width of nozzle exit respectively.

2.3 Boundary Conditions

Figure 4 shows boundary conditions in the present study. Mirror boundary condition is assumed at the nozzle axis. Non-slip and isothermal conditions are assumed on the wall. Also zero pressure gradient normal to the wall is assumed on the wall.

The total pressure and total temperature are assumed at the upper exit and velocity normal to the boundary is extrapolated by using inner points. Outflow condition is assumed at the external exit of the nozzle flow.

Gas constant and specific heat ratio are estimated by assuming a working fluid as combustion gas of hydrogen and oxygen.

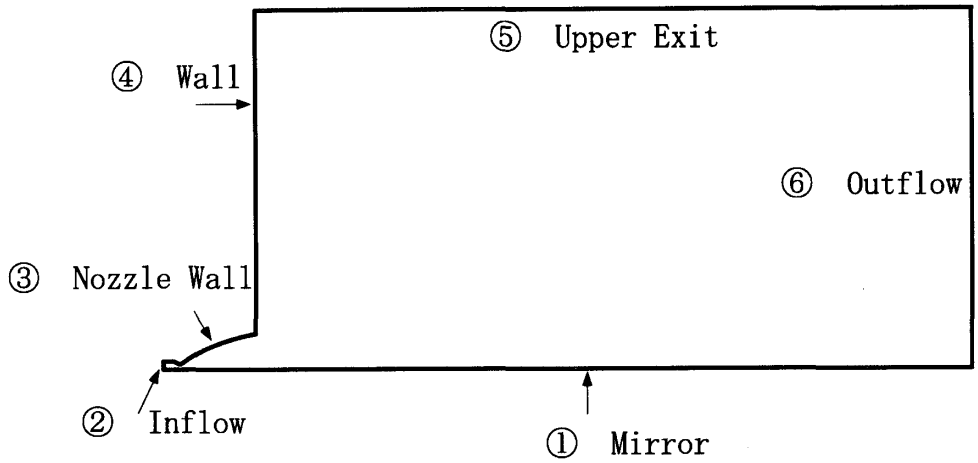

Fig. 4 Boundary conditions

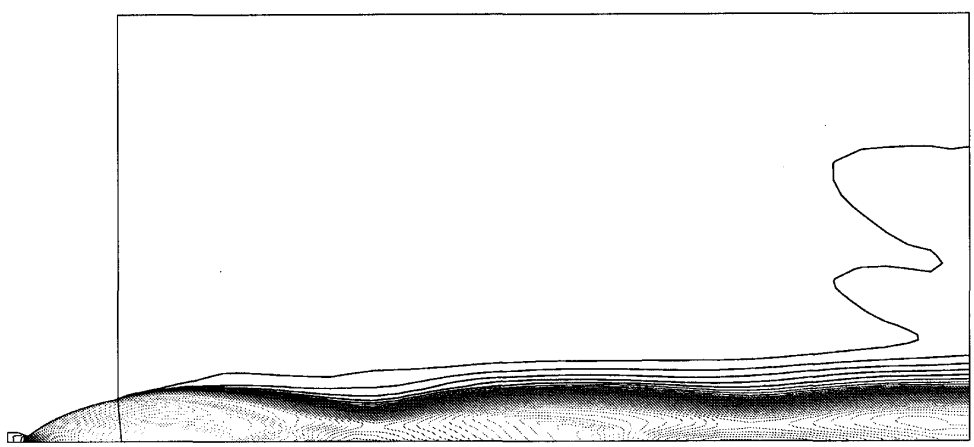

Fig. 5 Mach contours at PR=385

3. Results and Discussion

3.1 Steady Nozzle Flows

At first numerical simulations of nozzle flows at the pressure ratio, $PR = p_c/p_a$ where p_c is total pressure of combustion chamber and p_a is ambient pressure, of 385 and 770. Therefore $PR = 385$ is a half of design pressure ratio. Mach number contours of both cases are shown in **Figs. 5** and **6**. In both cases any separation is not observed in the nozzle and outer flow goes smoothly downstream.

3.2 Unsteady Calculation

In order to observe unsteady flow properties of the nozzle numerical simulations of starting process is conducted. In the calculations temporal change of chamber pressure (i.e. total pressure of combustion chamber) is assumed as in **Fig. 7**. The temporal change of chamber pressure is similar to the actual starting process of a rocket engine.

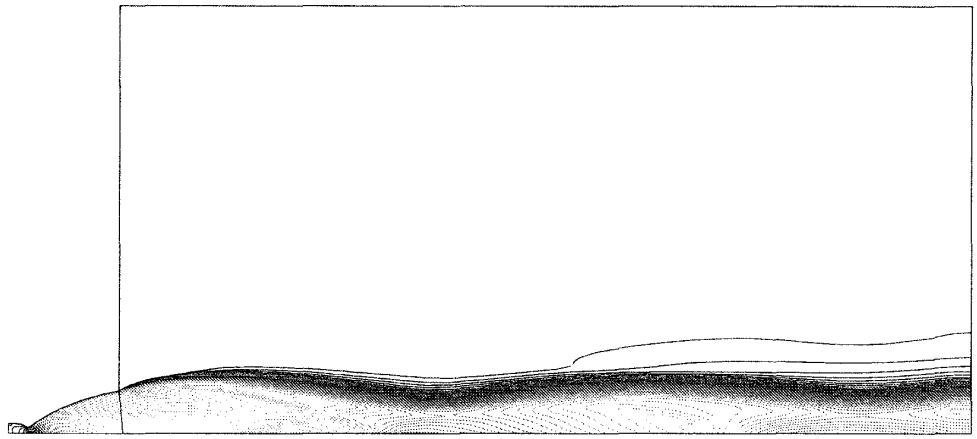

Fig. 6 Mach contours at PR=770

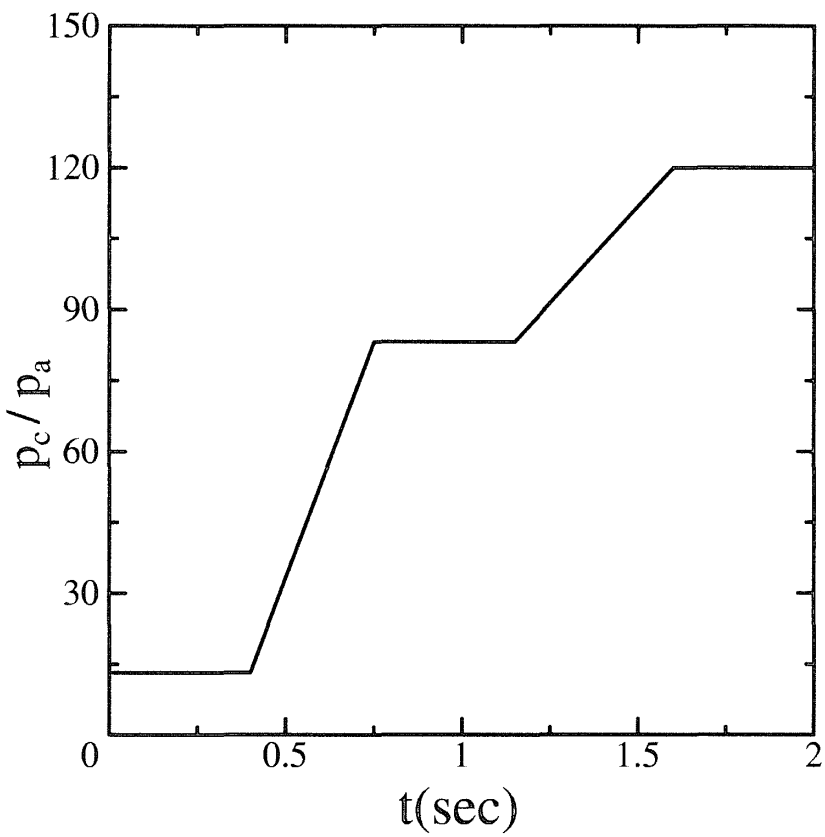

Fig. 7 Temporal change of chamber pressure

3.2.1 Estimation of Lateral Force from Calculated Results

Since the flow is assumed to be axisymmetrical, lateral force cannot be obtained from calculated results. In the actual nozzle flow the flow separates asymmetrically with some disturbance and the asymmetrical flow separation generates non-uniform pressure distribution inside the nozzle and this results in lateral force of the nozzle. In the present study in order to estimate the order of the magnitude of the lateral force of half of the nozzle

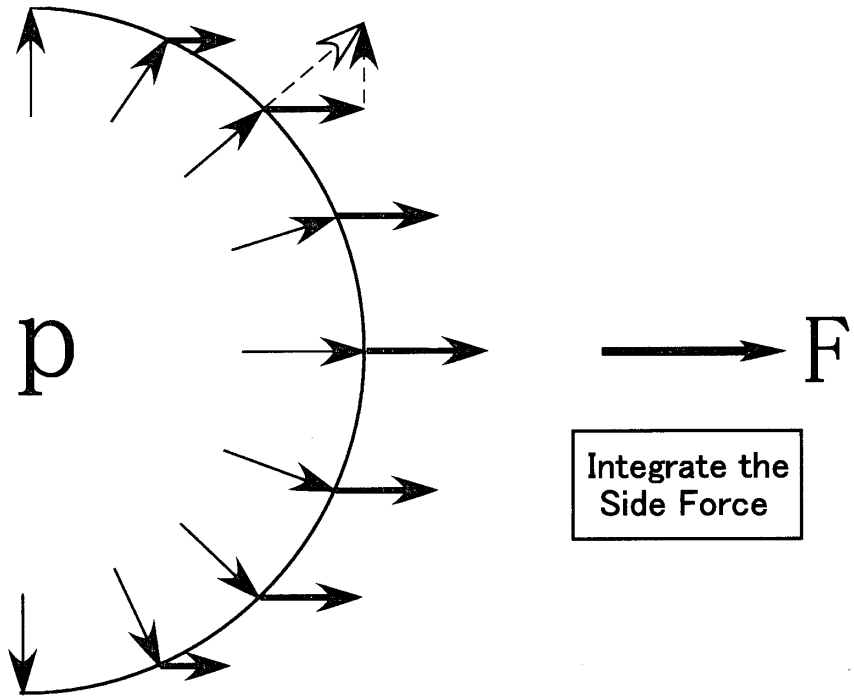

Fig. 8 Estimation of the lateral force

block, which is refered as F, is calculated as shown in the **Fig. 8**. The lateral component of pressure force acting on inside of the nozzle wall are integrated over the half surface of the nozzle and the integrated lateral pressure force is referred as lateral force of the nozzle, F. From now on the present authors call F as " lateral force" in the present paper.

3.2.2 Unsteady Flow Properties and Lateral Force at T_w=700K

The temporal change of lateral force at $T_w = 700$ K is shown in **Fig. 9**. The temporal change of chamber pressure is also shown in the Figure. In the Figure unsteady fluctuation of the lateral force begins to observe near $t = 1.25$ sec.

The temporal changes of pressure ratio, PR, lateral force and separation point, X, are shown in **Fig. 10**. As shown in the Figure, although PR is increased linearly between $t = 1.2$ sec and 1.6 sec, the separation point moves to downstream suddenly about 0.6 m before $t = 1.2$ sec and begins to move back and forth after $t = 1.2$ sec. Then, the separation point gradually moves to downstream. And after PR is reached to the final value, the separation point remains almost at the same position.

Characteristics of unsteady flow fields between $T = 1.2$ sec and $T = 1.4$ sec are investigated carefully in detail. The close-up of **Fig. 9** between $t = 1.15$ sec and $t = 1.45$ sec are shown in **Fig. 11**. And typical flow patterns of Mach contours and instantaneous stream lines near the nozzle exit of **Fig. 11** are shown in **Fig. 12** and **Fig. 13**. In the Figures the number of each flow pattern is related to the number indicated in the **Fig. 11**. And also flow categories of FSS and RSS are indicated in the Figures.

As shown in the Figures various flow patterns are observed and those flow patterns are identified as FSS or RSS. The lateral force shows minimum values at (1) ($t = 1.17$ sec), (3) ($t = 1.27$ sec) and (6) ($t = 1.37$ sec) and maximum values at (2) ($t = 1.22$ sec), (4) ($t = 1.30$ sec) and (5) ($t = 1.35$ sec).

At (1) ($t = 1.17$ sec) the flow is in FSS and separated flow moves almost parallel to the nozzle axis. At (2) ($t = 1.22$ sec) the vortex behind the Mach disk becomes large and the

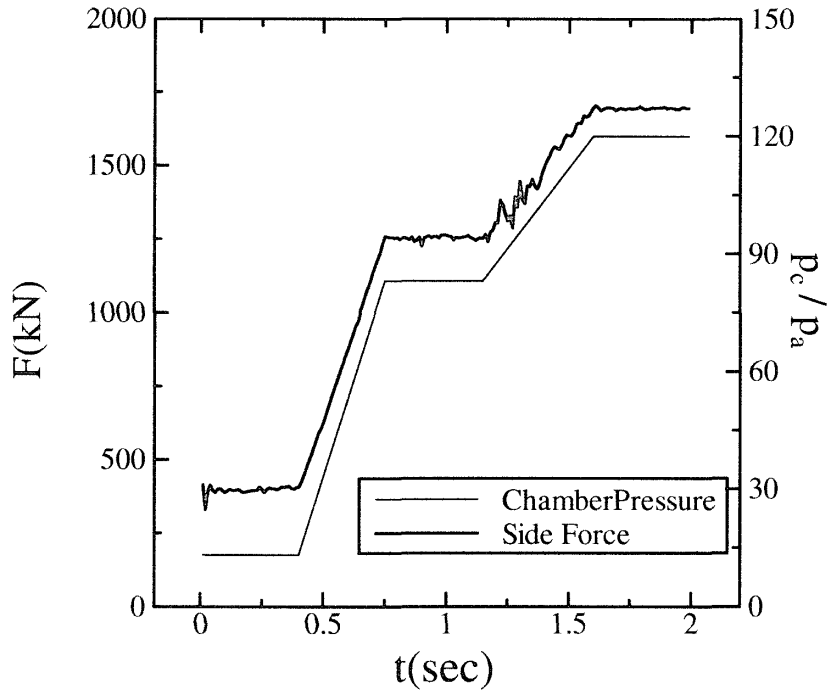

Fig. 9 Temporal change of lateral force and chamber pressure at $T_w = 700$ K

vortex makes the separated flow reattach just after separation and flow along the nozzle wall. At (3) ($t = 1.27$ sec) the separation point moves to almost the end of the nozzle and the reattachment point separates from nozzle exit. Since the separation regions of (1) and (3) are connected to ambient pressure. Minimum lateral forces are observed.

Between (4) ($t = 1.30$ sec) and (5) ($t = 1.35$ sec) Mach disk and a large vortex behind the Mach disk are observed and the large separated vortex moves to downstream and after that a vortex of opposite rotation is observed ((5)). After that quite complicated flow patterns with FSS are observed between (6) and (8).

After (8) ($t = 1.40$ sec) the flow becomes stable and show FSS flow patterns with large vortex behind Mach disk as same as (1).

Representative surface pressure distributions in FSS and RSS are shown in **Fig. 14** and **Fig. 15**. In FSS surface pressure increases after separation point. However it does not exceed ambient pressure. On the other hand in RSS surface pressure increases after separation point and the pressure level exceeds ambient pressure downstream of reattachment point. The increased pressure level is sometimes more than two times of ambient pressure and the higher pressure level is major reason of the generation of strong lateral force of the nozzle in starting process. As already shown in the **Fig. 11**. The maximum peak-to-peak value of fluctuation of lateral force, F, is about 120 kN. Which is quite enough order of magnitude of lateral force to deform the nozzle shape or to destroy the supporting system of the nozzle if flow separation in the nozzle is very asymmetry.

When PR is increased to the design pressure ratio, the flow becomes stable and flow pattern is in FSS. Strong lateral force is not observed in the flow condition.

Also it should be noted that strong lateral force will be generated when reattachment point moves downstream over the end of the nozzle in RSS. This is called as "end effects".

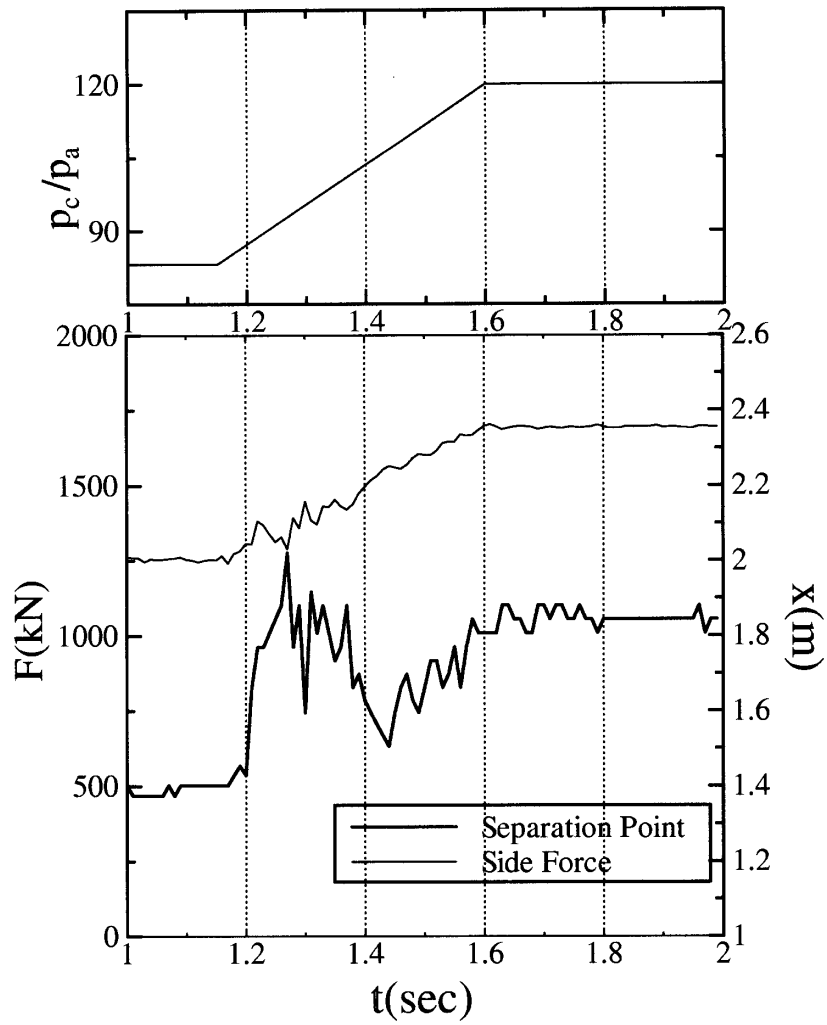

Fig. 10 Temporal change of pressure ratio, F and separation point (T_w = 700 K)

3.2.3 Unsteady Flow Properties and Lateral Force at T_w = 290 K

The time history of lateral force at T_w = 290 K is shown in **Fig. 16**. The temporal change of chamber pressure is also shown in the figure. Although F increases with the increase of chamber pressure, larger fluctuation is observed where PR is fixed constant. The fluctuation of F disappears when PR is increased again.

The temporal changes of pressure ratio, PR, lateral force and separation are shown in **Fig. 17**. As shown in the Figure, larger fluctuation is observed when PR is reached to a constant pressure ratio. And the fluctuation of F disappears when PR is increased over a constant pressure ratio. The fluctuation of separation point is also observed at a constant pressure ratio. The separation point moves to downstream gradually and stays at about $x = 2m$ when PR is reached to the design level. In T_w = 700 K the separation point stays at about x= 1.8 m when PR is reached to the design level. The global changes of fluctuation of lateral force and final separation point at design PR level with wall temperature show that the influences of surface temperature to the lateral force and unsteady flow characteristics are large.

The reason why the fluctuation of lateral force appears earlier in case of T_w =290 K compared with in case of T_w = 700 K for the same PR increase profile is as follows: A Sonic

line in a boundary layer moves closer to the wall when wall temperature decreases. Then the width of subsonic region where information from downstream could be transmitted becomes narrow and a separation point moves downstream rapidly and reaches to x= 1.8m at T_w= 290 K compared with in case of T_w = 700K.

In the present simulations quite different unsteady flow patterns are observed when nozzle wall temperature is changed from T_w = 700 K to T_w =290 K. Since flow separation is partly influenced by nozzle wall temperature quite difference unsteady flow fields are sometimes observed by changing the nozzle wall temperature.

In the present calculation conditions PR is kept constant between t = 0.75 sec and t = 1.15 sec. And unsteady flow patterns of FSS and RSS appear irregularly in the nozzle configuration used in the present calculation at x= about 1.8m. At T_w = 700 K separation point reaches to x = 1.8 m when PR is increased over a constant PR and strong fluctuation of lateral force is observed. At T_w = 290 K separation point reaches to x = 1.8 m just after PR is increased to a constant PR and strong fluctuation of lateral force is observed.

It is quite important to predict the location of separation point where FSS and RSS appeares irregularly in the nozzle design. And if PR have to be kept constant for some interval in the starting process with some thermal problems the constant PR level should be selected carefully in order to avoid the separation point of boundary layer of nozzle flow not to reach the location of separation point where FSS and RSS appears irregularly.

3.2.4 Effect of Temporal Profile of Chamber Pressure to the Design Level on Unsteady Flow Properties

The effect of temporal profile of chamber pressure to the design level on unsteady flow properties are investigated. The fluctuations of lateral force during the various increase process of the chamber pressure are observed. In the Figure the profile (1) shows quick increase of chamber pressure to the design pressure ratio and the profile (2) shows slow increase of chamber pressure to the design pressure ratio.

The temporal change of lateral forces of both cases are shown in **Fig. 19**. In the profile of (1) fluctuations of lateral force are not observed except PR = about 90. In the profile of (2) strong fluctuations of lateral force are observed where x is about 1.8m. The results show unsteady flow patterns and strong fluctuation of lateral force occur when separation point reaches at x =1.8 m for the present nozzle configuration.

Also the results show that rapid increase of chamber pressure is recommended in order to avoid strong fluctuations of lateral force.

4. Conclusions

The conclusions in the present study are summaried as follows:

1. The unsteady flows in the starting process of the Bell-type nozzle configuration have been simulated by increasing chamber pressure ratio, PR. When PR is increased in the present nozzle configuration, unsteady flow patterns are observed and both flow patterns FSS (Free Shock Separation) and RSS (Restricted Shock Separation) are observed. Especially in RSS higher pressure region is observed in the separated region. The increased pressure level is sometimes more than two times of ambient pressure and the higher pressure level is major reason of the generation of strong lateral force of the nozzle in starting process if wide asymmetry separation occurs.

2. The maximum peak-to-peak value of fluctuation of lateral force, F, is about 120 kN.

Which is quite enough order of magnitude of lateral force to deform the nozzle shape or to destroy the supporting system of the nozzle if flow separation in the nozzle is very asymmetry.

3. In the present simulations quite different unsteady flow patterns are observed when nozzle wall temperature is changed from T_w =700 K to T_w 290 K. Since flow separation is partly influenced by nozzle wall temperature, quite different unsteady flow fields are sometimes observed by changing the nozzle wall temperature.

4. In the nozzle design it is quite important to predict the location of separation point where FSS and RSS appears irregularly. And if PR have to be kept constant for some interval in the starting process with some thermal problems the constant PR level should be selected carefully in order to avoid the separation point of boundary layer of nozzle flow not to reach the location of separation point where FSS and RSS appears irregularly.

5. The effects of temporal profile of chamber pressure to the design level on unsteady flow properties are investigated. The fluctuations of lateral force during the various increase process of the chamber pressure are observed. The results show that rapid increase of chamber pressure is recommended in order to avoid strong fluctuations of lateral force.

References

1) M. Onofri and F. Nasuti : The Physical Origins of Side Loads in Rocket Nozzles, AIAA 99-2587 (1999).
2) L. H. Nave and G. A. Coffey : Sea Level Side loads in High-Area-Ratio Engines, AIAA 73-1284 (1973).
3) M. Frey and G. Hagemann : Status of Flow Separation Prediction in Rocket Nozzles, AIAA 98-3619 (1998).
4) M. Frey and G. Hagemann : Restricted Shock Separation in Rocket Nozzles, J. of Propulsion and Power, Vol. 16, No. 3 (2000), pp. 478-484.
5) C. L. Chen, S. R. Chakravarthy and C. M. Hung : Numerical Investigation of Separated Nozzle Flows, AIAA J., Vol. 32, No. 9 (1994), pp. 1836-1843.
6) G. V. R. Rao : Exhaust Nozzle Contour for Optimum Thrust, J. of Jet Propulsion, June 1958 (1958), pp.377-382.
7) J. D. Hoffman : Design of Compressed Truncated Perfect Nozzles, AIAA 85-1172 (1985).

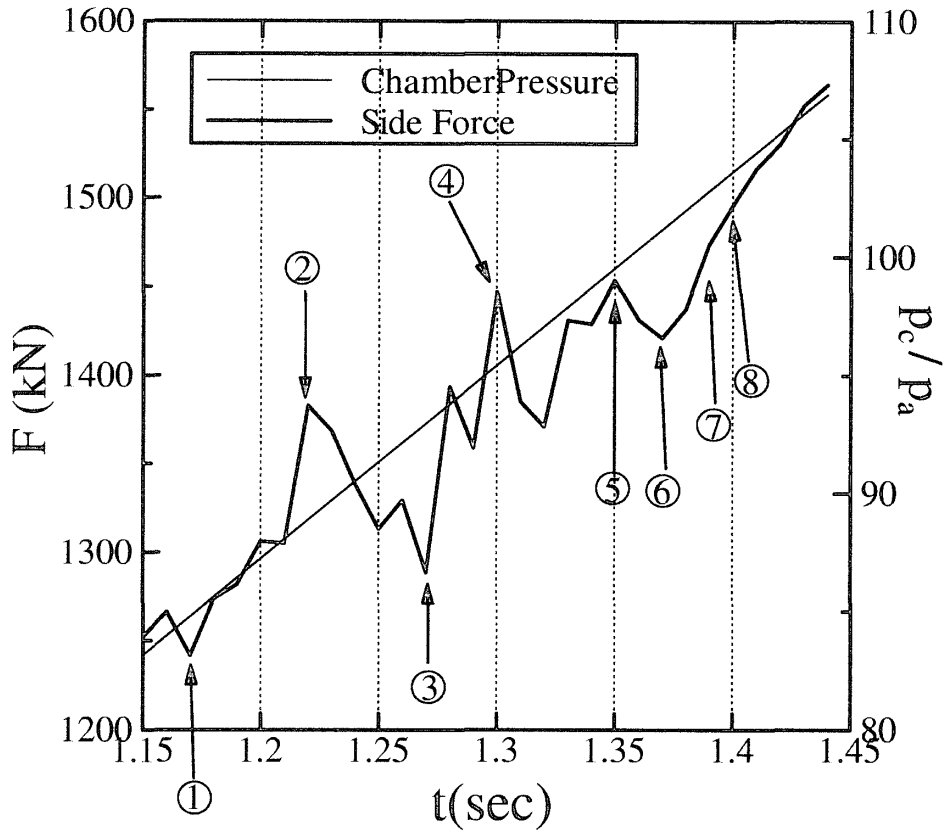

Fig. 11 Temporal change of pressure ratio and between $t = 1.15$ sec and $t = 1.45$ sec ($T_w = 700$ K)

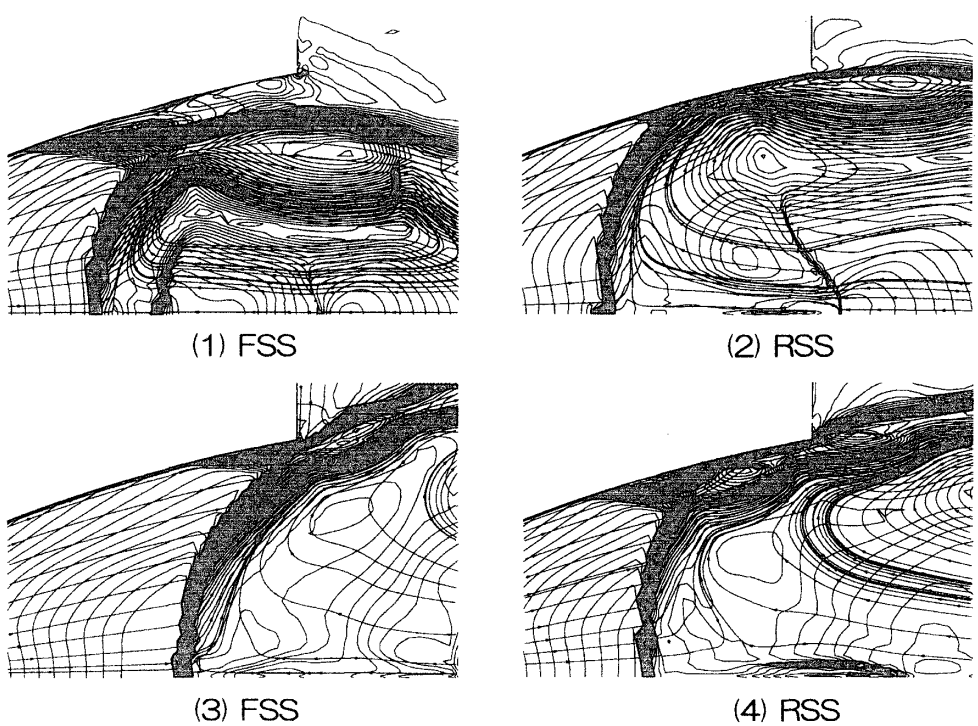

Fig. 12 Typical flow patterns of Mach contours and instantaneous stream lines near the nozzle exit ((1)-(4)) ($T_w = 700$ K)

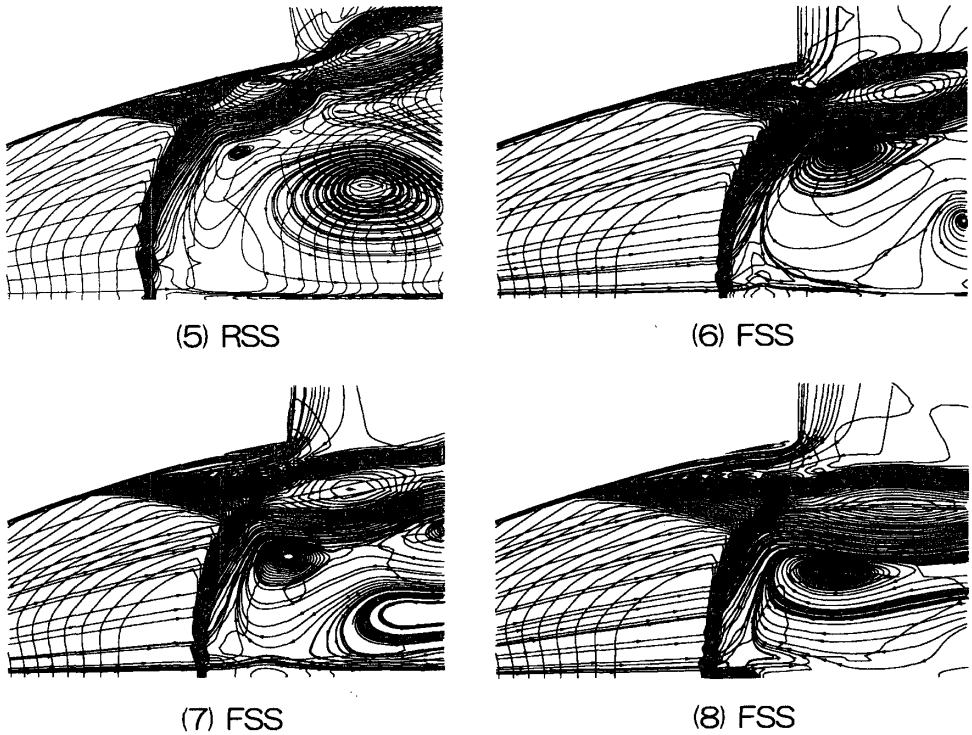

Fig. 13 Typical flow patterns of Mach contours and instananeous stream lines near the nozzle exit ((5)-(8)) (T_w = 700 K)

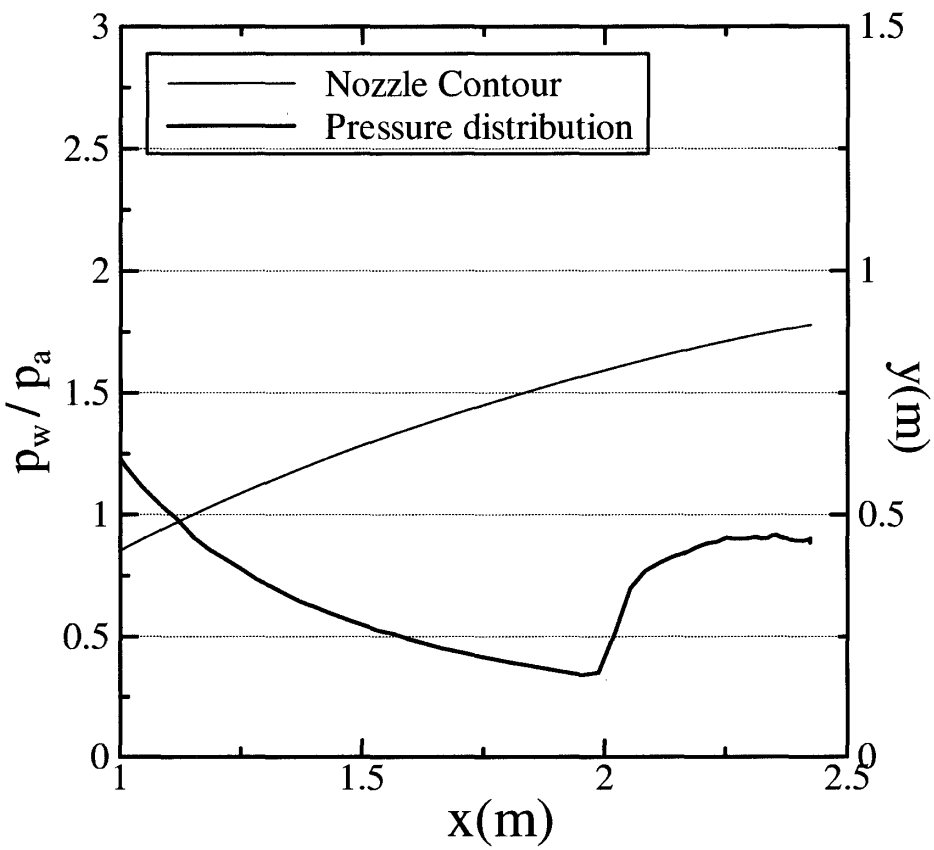

Fig. 14 Representative surface pressure distribution in FSS ((1) of **Fig. 12**)

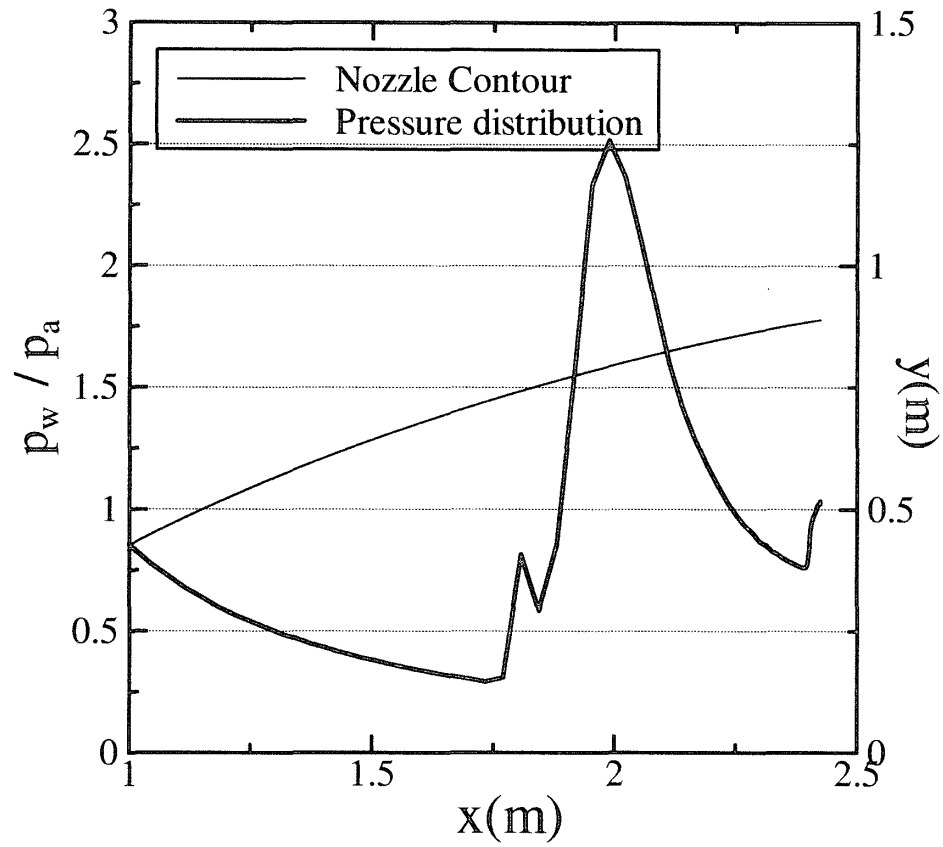

Fig. 15 Representative surface pressure distribution in RSS ((4) of **Fig. 12**)

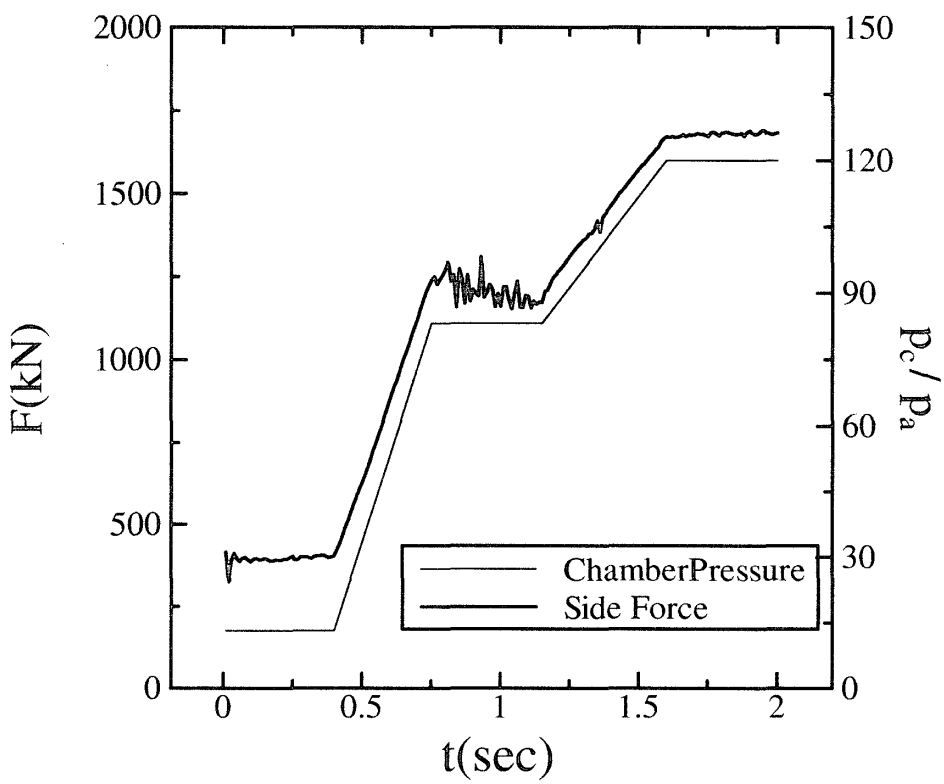

Fig. 16 Temporal change of lateral force and chamber pressure at $T_w = 290$ K

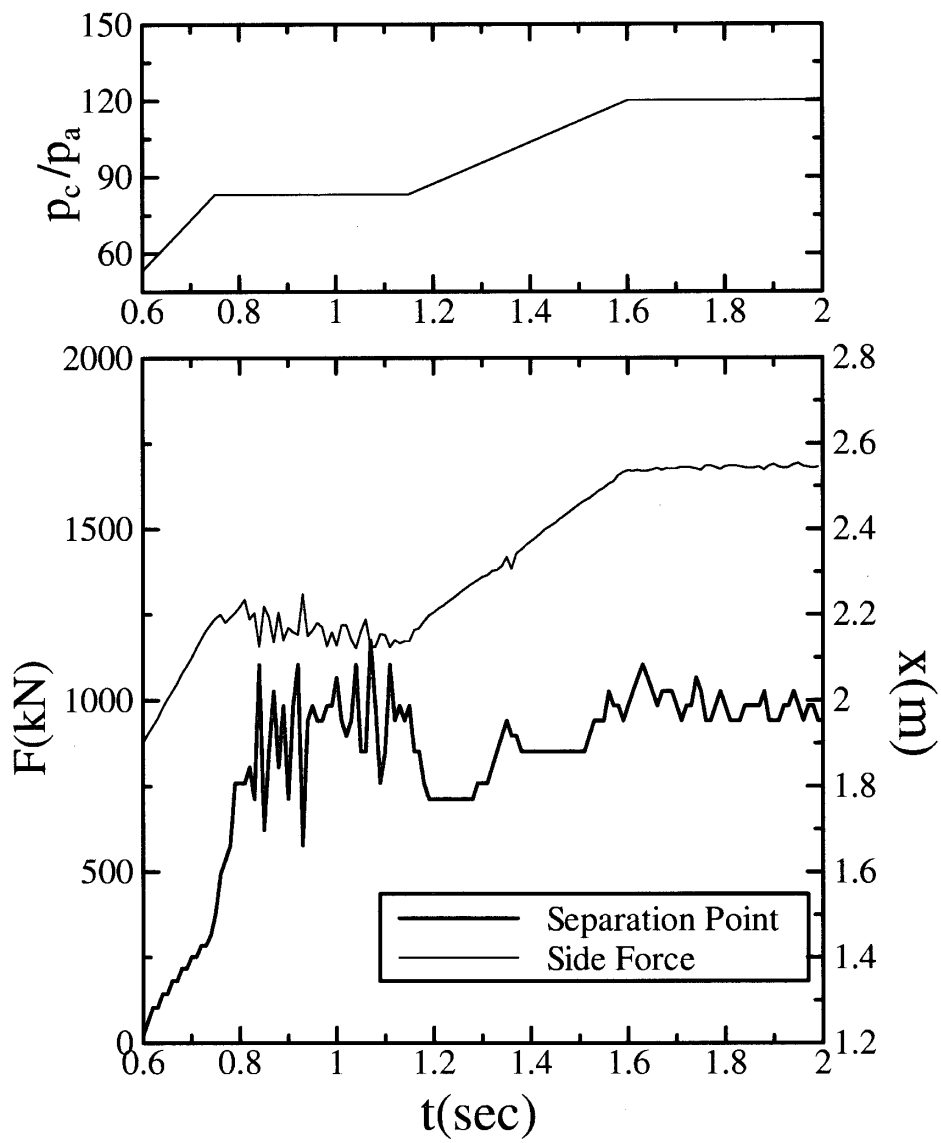

Fig. 17 Temporal change of pressure ratio, F and separation point (T_w = 290 K)

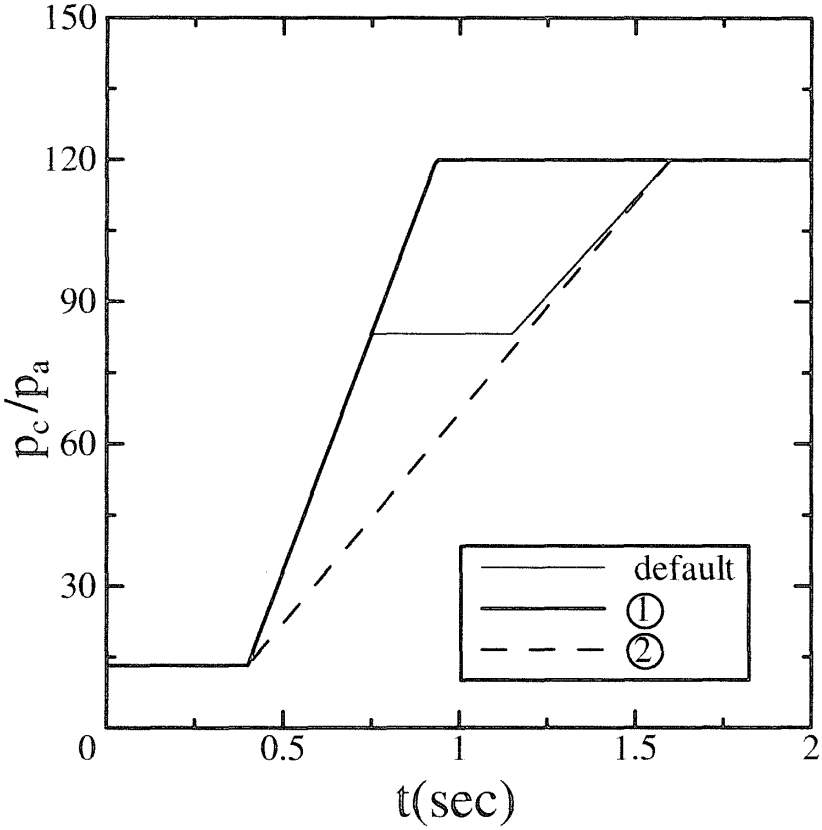

Fig. 18 Two kinds of temporal changes of chamber pressure

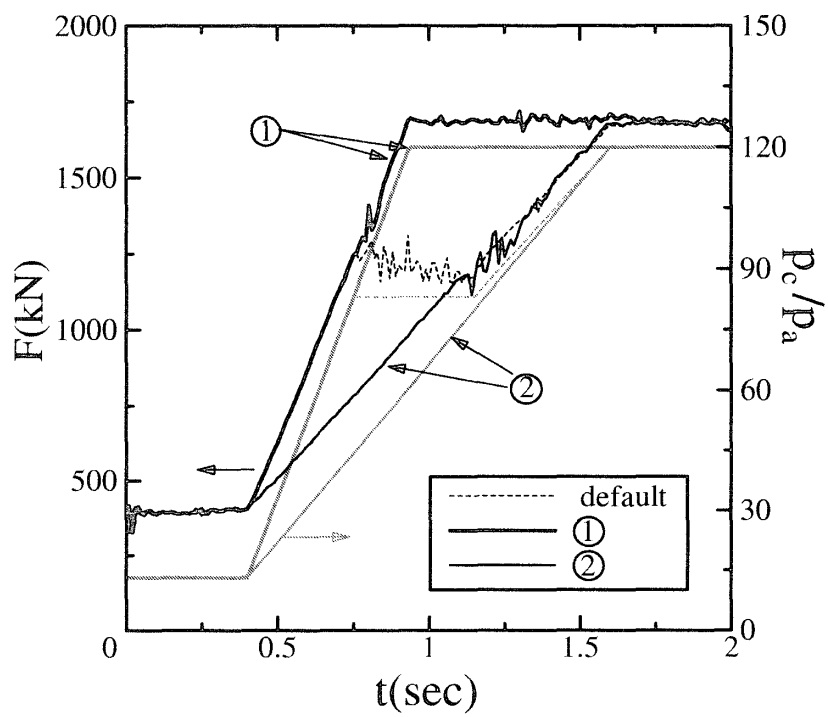

Fig. 19 Temporal changes of lateral forces under various conditions